Journal of Polymer Research (2019) 26: 5
https://doi.org/10.1007/s10965-018-1650-z

ORIGINAL PAPER

# Ultralow-dielectric, nanoporous poly(methyl silsesquioxanes) films templated by a self-assembled block copolymer upon solvent annealing

C. Wang [1] · T. M. Wang [1] · Q. H. Wang [1]

Received: 24 April 2018 / Accepted: 6 November 2018 / Published online: 6 December 2018
© Springer Nature B.V. 2018

## Abstract

A homogenous, nanoporous poly(methyl silsesquixoxane) (PMSSQ) with a uniform pore size distribution was prepared by templating with a poly(styrene-b-4-vinylpyridine) (PS-*b*-P4VP) block copolymer. The self-assembly of the PS-*b*-P4VP and PMSSQ precursor (PMSSQ-P) blends thin films was achieved by solvent annealing firstly; then the self-assembled thin films were thermally cured to prepare nanoporous PMSSQ films after removal of the PS-*b*-P4VP porogen. The influence of annealing solvent and PS-*b*-P4VP loading on the self-assembly behavior of the PS-*b*-P4VP/PMSSQ-P blends films were studied. By exposing to $CHCl_3$ vapor, fingerprint-type microphase-separated structures were achieved for the PS-*b*-P4VP/PMSSQ-P blends films with PS-*b*-P4VP loading ranging from 30% to 60%. The formation of the microphase-separated structures is attributed to the substantial mobility of the PS blocks and the P4VP/PMSSQ-P complexes, and segregated repulsion between them under the $CHCl_3$ vapor. Atomic force microscopy (AFM), scanning electron microscopy (SEM), and transmission electron microscopy (TEM) results demonstrated the prepared nanoporous PMSSQ films had a homogenous spherical pore morphology, with closed nanopores and a uniform size distribution over large areas. The porosity and dielectric properties of the homogenous, nanoporous PMSSQ could be adjusted by the content of PS-*b*-P4VP in the PS-*b*-P4VP/PMSSQ-P blends. As the PS-*b*-P4VP loading increased to 60 wt%, an ultralow dielectric constant of 1.41 was obtained, making the nanoporous PMSSQ films have potential applications in microelectronic devices.

**Keywords** Block copolymers · Dielectric constant · Nanoporous · Poly(methyl silsesquixoxane) · Solvent annealing

## Introduction

According to the international technology roadmap for semiconductors, the feature dimension in integrated circuits will shrink to ca. 6 nm around year 2026 [1]. Rapid development of microelectronics requires integrated circuits with higher clock speeds, reduced geometries and increased wiring densities, all of which lead to increased resistance and capacitance delays. This necessitates the use of low dielectric constant ($k$) materials as interlayer dielectrics to reduce crosstalk and parasitic capacitance between adjacent interconnects [2–4]. However, traditional dielectric interlayers, like silica oxide with a high dielectric constant of 4.0, do not meet the requirement; as a result the search for low- or ultralow-$k$ (low-$k$: $k \leq 2.5$; ultralow-$k$: $k \leq 2.0$) materials has been extensive and pervasive within both industry and academia to fulfill the need for smaller feature size of technology nodes [5, 6].

Low-$k$ materials must also possess good thermal, chemical and mechanical properties in addition to the low dielectric permittivity [7]. Among the several potentially applicable dielectric materials, poly(methyl silsesquioxanes) (PMSSQ) are the most promising matrix material, due to the low polarizability of the Si-C methyl group, giving rise to its low dielectric constant (2.1~2.7), while exhibiting superior thermal stabilities (>500 °C), and has been extensively researched [8, 9]. The incorporation of nanopores filled with air ($k$~1.0) into the PMSSQ matrix is a technique widely used to further reduce the $k$ value of PMSSQ thin films. One promising approach is the templated polymerization of PMSSQ precursors (PMSSQ-P) in the presence of thermally labile organic porogens, and subsequently creating pores through the sacrificial thermal decomposition of the porogens. Except dendrimers [10, 11], star-shaped polymers [12, 13], nitrogen containing copolymer

✉ C. Wang
wangc@licp.cas.cn

[1] State Key Laboratory of Solid Lubrication, Lanzhou Institute of Chemical Physics, Chinese Academy of Sciences, Lanzhou 730000, People's Republic of China

and hyperbranched polymers [14, 15] and amphiphilic block copolymers such as PEO-PPO-PEO [16, 17], PS-*b*-PMSMA [18], PS-*b*-P2VP [19, 20] and PS-*b*-P4VP [21], have been shown to be effective porogens and are commonly used to prepare nanoporous PMSSQ. These block copolymers can be self-assembled into versatile nanoscale morphologies, which could be "duplicated" and "transformed" to porous PMSSQ based on the interpolymer interaction between the block copolymers and PMSSQ-P. Therefore, the pore size, pore shape, and porous structure regulation of the PMSSQ could be precisely adjusted by the block copolymers [19, 20].

The formation of self-assembly nanostructures of the block copolymer in the PMSSQ-P matrix was the precondition of fabrication of the porous PMSSQ [16–21]. To the best of our knowledge, the previously reported microphase-separated structures were obtained in-situ during the thermal curing of spin-coated thin films of mixtures of PMSSQ-P and a block copolymer. Therefore, the size distribution and arrangement of the microphase-separated structures were usually inhomogeneous, thus generating randomly shaped large pores, and even interconnected pores. For use in integrated circuits with small feature sizes, it is necessary to generate closed nanopores with a pore size much smaller than the feature size and a uniform size distribution [11, 22].

In this study we addressed a new way to prepare homogenous, nanoporous PMSSQ thin films with closed nanopores and a uniform pore size distribution using a block copolymer as template. Different from the traditional block copolymer template method, ordered and oriented self-assembled thin films were firstly obtained by solvent annealing; then the self-assembled thin films were thermally treated to complete the curing of the PMSSQ-P and, after pyrolysis of the block copolymer, nanoporous PMSSQ films were obtained. Compared to the porous PMSSQ films in previous report, the prepared nanoporous PMSSQ films have uniform spherical pore morphology and closed nanoscale pores; in addition, they appeared quite homogenous over large areas, without any large pores or other aggregation structures. The porosity and dielectric properties of the homogenous nanoporous PMSSQ could be adjusted by the PS-*b*-P4VP loading. When the PS-*b*-P4VP loading was increased to 60 wt%, an ultralow-*k* value of 1.41 was obtained.

## Experimental procedures

### Materials

All reagents were purchased from Tianjin Chemical Reagents Co., China, unless noted. PS-*b*-P4VP block copolymer ($M_n$ PS: P4VP = 11,800: 15000 g/mol and dispersity of 1.04) was purchased from Polymer Source Inc., Canada, and used as-received. Methyl trimethoxysilane (MTMS, Acros Organics, Belgium, 97%), hydrochloric acid (HCl, 37.5%), trichloromethane ($CHCl_3$), tetrahydrofuran (THF), ethanol, and benzene were analytical chemical reagents and used as-received.

### Synthesis of PMSSQ precursor (PMSSQ-P)

PMSSQ-P was synthesized according to a previous report [23]. The details are as follows: In a reaction flask fitted with a mechanical stirrer and Ar inlet, 6.8 g of MTMS and 10 g of THF were placed and cooled in an ice bath for 10 min; then 1.08 g distilled water and 0.152 g HCl were added. The mixture was stirred at room temperature for 10 min, followed by stirring at 60 °C for 3 h to yield a viscous PMSSQ-P solution.

The successful preparation of PMSSQ-P was verified by its FTIR spectra. The molecular weight and molecular weight distribution of PMSSQ-P were determined by GPC ($M_w$ = 2200,$M_n$ = 1220,$M_w/M_n$ = 1.8).

### Preparation of self-assembled PS-*b*-P4VP/PMSSQ-P thin films

The block copolymer PS-*b*-P4VP and PMSSQ-P were first individually dissolved in a THF/ethanol mixture, to make polymer solutions with concentrations of 2 wt%. Then, the two solutions were mixed with different weight content of PS-*b*-P4VP in the total solid ranging from 30% to 80% with 10 wt% intervals, and stirred for more than 24 h at room temperature. PS-*b*-P4VP/PMSSQ-P blends in films with thickness of ~100 nm, were prepared on a silicon wafer by spin-coating at 2000 rpm for 30 s, followed by drying under vacuum at room temperature to remove residual solvent. The as-spun PS-*b*-P4VP/PMSSQ-P films were solvent annealed in a saturated solvent vapor of $CHCl_3$ at 25 °C to achieve self-assembled microstructures.

The solvent annealing experiment is shown in Fig. 1. The thin films were placed in a totally air-tight vessel along with a 50 ml volume open vial containing solvent. The environment outside the vessel was maintained at 25 °C; after solvent annealing for 24 h, the films were removed from the vessel quickly and air-dried at room temperature.

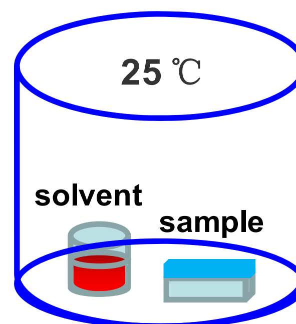


**Fig. 1** Schematic diagram of solvent annealing equipment

### Preparation of nanoporous PMSSQ thin films

The self-assembled PS-*b*-P4VP/PMSSQ-P films and spin-cast PS-*b*-P4VP/PMSSQ-P films without solvent annealing were thermally treated to convert the PMSSQ-P to PMSSQ at an elevated temperature: 25 °C (0.5 h), 50 °C (0.5 h), 80 °C(0.5 h), 100 °C (1 h), and 120 °C (12 h), sequentially. The nanoporous PMSSQ films, with thicknesses of ~100 nm, were obtained after the removal of the PS-*b*-P4VP block copolymer by thermal decomposition at 350 °C and 450 °C, successively, for 0.5 h at each temperature.

### Characterization

AFM studies were conducted with a Nanoscope IIIa multimode atomic force microscope (VEECO Digital Instrument, USA) in the tapping mode. SEM images were obtained with a JSM-6701F field emission scanning electron microscope (JEOL Ltd., Japan). All samples were coated with gold by sputtering prior to observation. A JEM 2010 transmission electron microscope (JEOL Ltd., Japan), operating at an accelerating voltage of 200 kV, was used to examine the morphology of the nanoporous PMSSQ films. Thin Films of similar thickness for TEM were prepared on NaCl substrates. These films were floated onto the surface of deionized water after dissolution of the NaCl, and then picked up by a carbon film covered Cu grid. The FTIR spectra were measured using a IFS 66 V/S FTIR spectrometer (Bruker Co., Germany) within a range of 4000–400 $cm^{-1}$. DSC analysis was conducted with a DSC $822^e$ (Mettler-Toledo Instrument, Swiss), with a heating or cooling rate of 10 °C/min. The sample was heated to 200 °C and kept at this temperature for 5 min, cooled to 25°Cin order to remove the thermal history; the sample was then heated to 200 °C again to obtain the DSC data. GPC analysis was performed using a Gel Permeation Chromatography system (Waters Co., USA). THF was used as an eluent, and the results were calibrated with respect to polystyrene standards. Thermogravimetry analysis was conducted with a STA 449 C TG-DSC thermogravimeter (NETZSCH Group, Germany) at a heating rate of 10 °C/min in nitrogen atmosphere. The porosity ($V$) of the nanoporous PMSSQ thin films was obtained from the refractive index according to the Lorentz–Lorenz equation, as follows [24]:

$$V = 1 - \left[ \frac{\left(n_p^2 - 1\right)\left(n_s^2 + 2\right)}{\left(n_p^2 + 2\right)\left(n_s^2 - 1\right)} \right] \tag{1}$$

Where $n_p$ and $n_s$ are the refractive indices of the nanoporous and dense PMSSQ thin films, respectively. The dielectric constants of the nanoporous PMSSQ films were determined using the Maxwell equation [25]:

$$\varepsilon \cong 1.1 \times n^2 \tag{2}$$

where $n$ is the refractive index. The refractive index was measured with a variable-angle multi-wavelength L116E ellipsometer (Gaertner Ltd., USA) with a wavelength of 632.8 nm.

## Results and discussion

As previously reported, the synthesized PMSSQ-P has abundant hydroxyl groups which can form strong hydrogen-bonds with the pyridine nitrogen atoms of the P4VP blocks to form P4VP/PMSSQ-P complexes, which could increase the miscibility between PMSSQ-P and PS-*b*-P4VP, avoiding macrophase separation in PS-*b*-P4VP/PMSSQ-P blends thin films [21]. Furthermore, the selective adsorption of PMSSQ-P on the P4VP blocks not only enhanced the segregated repulsion between the PS and P4VP blocks, but could also possibly change the self-assembly structure of the pure PS-*b*-P4VP by increasing the volume fraction of P4VP domains relative to that of the domains of the PS blocks [26–28]. Table 1 lists the possible microphase-separated structures of PS-*b*-P4VP/PMSSQ-P blends with different weight content of PMSSQ-P, predicted from relative volume fractions of the PS blocks and P4VP/PMSSQ-P complexes according to the self-consistent mean field theory [29].

Solvent annealing, as a simple and effective way to control the microdomain orientation and long-range ordering in block copolymer thin films [30–33], was used to achieve the self-assembly of the PS-*b*-P4VP block copolymer and PMSSQ-P in the present study. Prior to discussion, it should be noted that the solvent annealing process was carried out at 25 °C, at which temperature the curing reaction of PMSSQ-P would not occur and thus avoided its influence on the self-assembly of the PS-*b*-P4VP/PMSSQ-P thin films. Figure 2a shows the AFM phase image of the spin-coated PS-*b*-P4VP/PMSSQ-P thin film blend with PS-*b*-P4VP loading of 50 wt%; a disordered microphase-separated morphology was formed. The AFM images, measured in the phase mode, shows the harder material as a bright color, while the softer material is a dark color [34]. Therefore, it could be concluded that the disordered structure consisted of P4VP/PMSSQ-P microdomains distributed in a PS matrix. The disordered microphase-separated structures are quite different from that predicted theoretically (see Table 1, spheres or cylinders), indicating the microphase-separated structures were in a trapped non-equilibrium state.

**Table 1** Composition and possible phase structure of the PS-*b*-P4VP/PMSSQ-P blends with different loading of PS-*b*-P4VP

| PS-*b*-P4VP wt% | Volume fraction | | Possible self-assembly structures [a] |
|---|---|---|---|
| | $\varphi_{PS}$ | $\varphi_{P4VP/PMSSQ-P}$ | |
| 30% | 0.14 | 0.86 | spheres |
| 40% | 0.19 | 0.81 | cylinders or spheres |
| 50% | 0.23 | 0.77 | cylinders or spheres |
| 60% | 0.27 | 0.73 | cylinders |
| 70% | 0.32 | 0.68 | lamellae |
| 80% | 0.36 | 0.64 | lamellae |
| 100% | 0.44 | 0.56 | lamellae |

[a] Possible thermodynamically stable self-assembly structures predicated from the relative volume fraction of PS blocks and P4VP/PMSSQ-P complexes according to the self-consistent mean field theory [29]

The underlying mechanism of solvent annealing has been well explained by pioneering researchers [30, 31, 34–36]. The resulting morphology and microphase-separated structures of block copolymer due to solvent annealing are mainly dependent on the nature/selectivity of the solvent. When an AB diblock copolymer are swelled by a solvent *C*, the effective interaction parameter will change [35]:

$$\chi_{eff} \cong \phi(\chi_{AB} + \Delta\chi) = \phi(\chi_{AB} + |\chi_{AC} - \chi_{BC}|) \tag{3}$$

where φ is the volume concentration of copolymer in the solvent and $\Delta\chi$ is the difference between the A-C and B-C

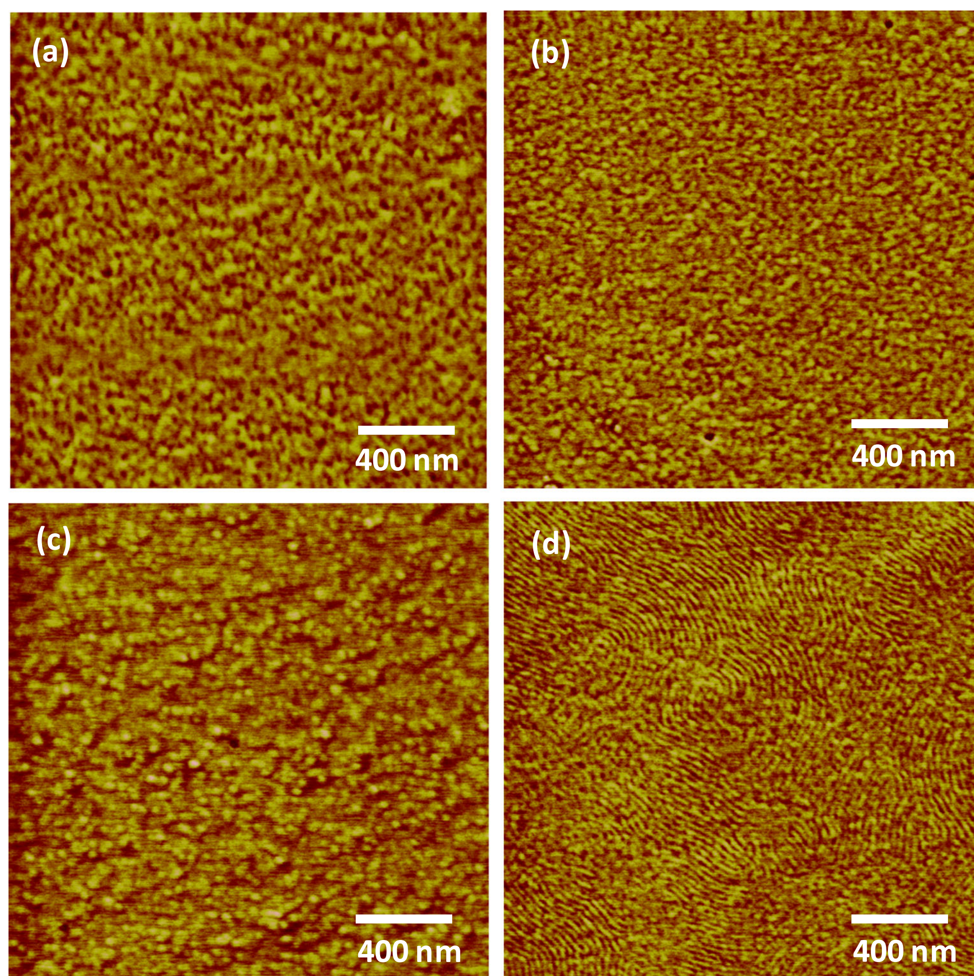


**Fig. 2** AFM phase images of PS-*b*-P4VP/PMSSQ-P thin film blends with PS-b-P4VP loading of 50 wt% (**a**) before and after solvent annealing in different solvent vapor: (**b**) ethanol; (**c**) THF; (**d**) $CHCl_3$

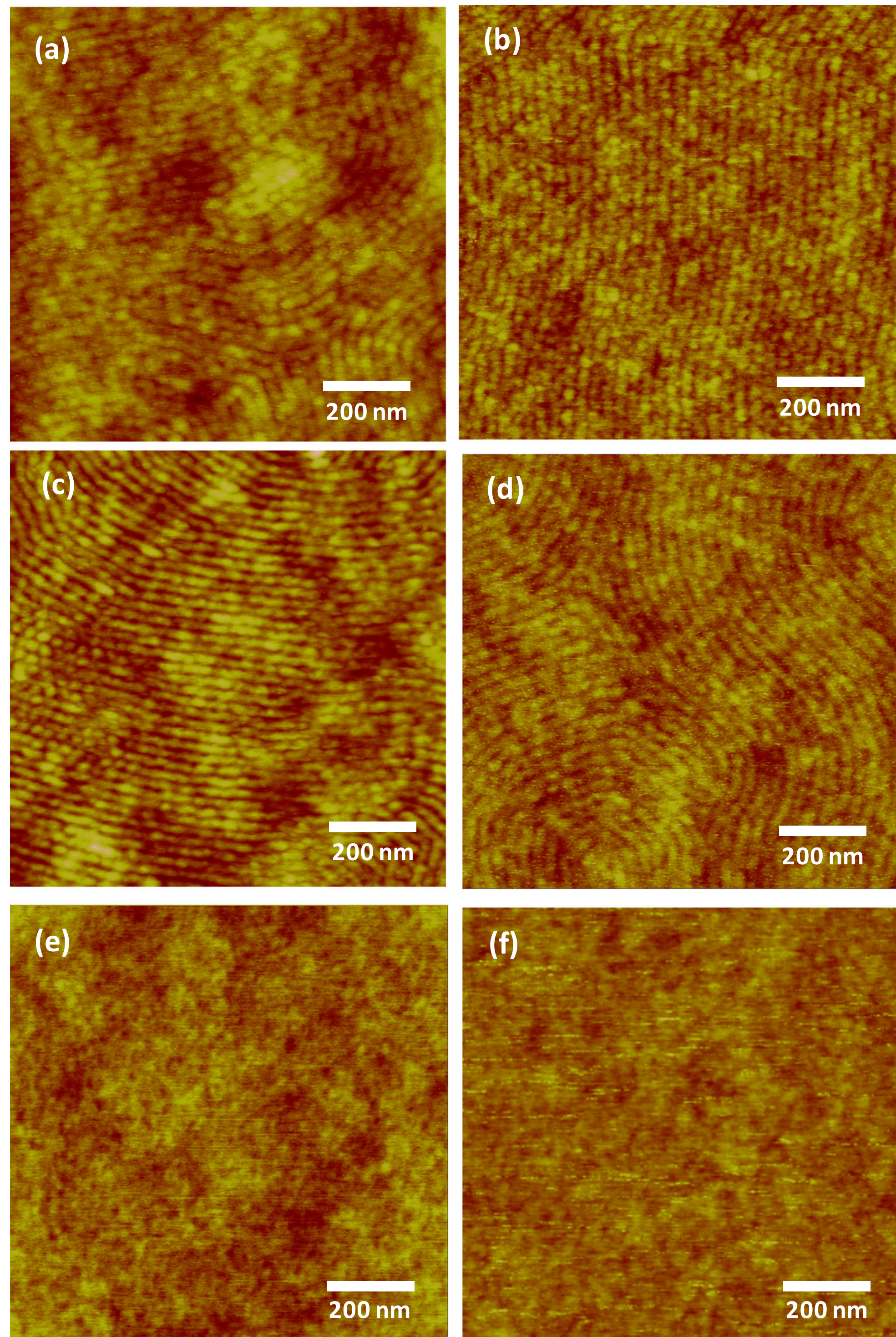


**Fig. 3** AFM height images of PS-*b*-P4VP/PMSSQ-P thin film blends with different PS-*b*-P4VP content after solvent annealing in $CHCl_3$ vapor. (**a**) 30 wt%, (**b**) 40 wt%, (**c**) 50 wt%, (**d**) 60 wt%, (**e**) 70 wt%, (**f**) 80 wt%

interaction parameters $\chi_{AC}$ and $\chi_{BC}$. Therefore, three different solvents, ethanol being a good solvent for only P4VP, THF being a PS selective solvent, and $CHCl_3$ being a non-selective solvent for the pure PS-b-P4VP block copolymer, were used to treat the PS-b-P4VP/PMSSQ-P blends thin films in the study. Figure 2b shows a AFM phase image of the PS-*b*-P4VP/PMSSQ-P thin films after annealing in ethanol. Compared to the spin-coated PS-*b*-P4VP/PMSSQ-P thin film (Fig. 2a), the morphology did not change obviously and showed a smaller domain structure for the films annealed in ethanol vapor (Fig. 2b). This is because ethanol is a good solvent for only the P4VP/PMSSQ-P complexes; the PS blocks could not migrate under the influence of ethanol vapor, thus leading to the inconspicous changes of the disordered

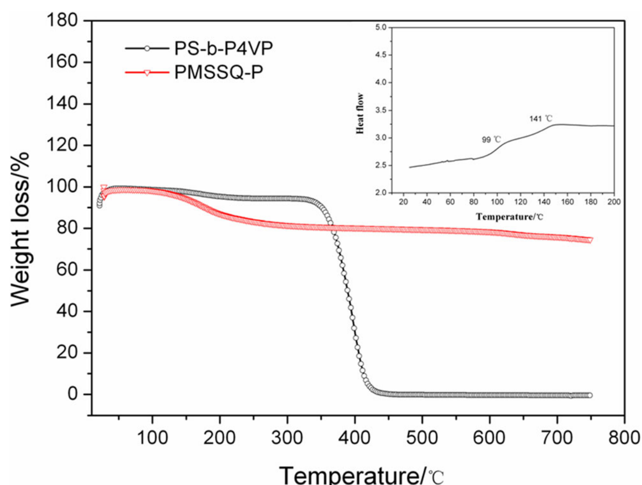


**Fig. 4** TGA curves of the pure PMSSQ-P and PS-*b*-P4VP block copolymer. Inset: DSC curve of PS-b-P4VP block copolymer, 99 °C and 141 °C are the glass transition temperature ($T_g$) of PS and P4VP blocks, respectively

microphase-separated structures. Figure 2c represents the morphology of PS-*b*-P4VP/PMSSQ-P thin films after annealing in THF; a spherical structure can be seen consisting of P4VP/PMSSQ-P microdomains distributed in a PS matrix. Although THF is only a slightly selective solvent for pure PS-*b*-P4VP, as previously reported [34, 37], selective adsorption of PMSSQ-P on the P4VP blocks increased the interaction parameter difference between PS and P4VP, making THF become highly selective for the PS blocks. The preferential affinity of THF for the PS blocks induced the formation of spherical microphase-separated structures with P4VP/PMSSQ-P complexes as cores and PS blocks as matrix. However, the spherical microphase-separated structures with P4VP/PMSSQ-P complexes as the cores were not suitable for the fabrication of nanoporous PMSSQ thin films by the pyrolysis of PS-*b*-P4VP. Figure 2d shows the AFM phase image of the PS-*b*-P4VP/PMSSQ-P thin films after annealing in $CHCl_3$. Fingerprint patterns of PS cylinders packed in oriented arrays parallel to the substrate in P4VP/PMSSQ-P matrix were obtained. Although the adsorption of PMSSQ-P on the P4VP blocks would also change the selectivity of $CHCl_3$, as occurred for THF, $CHCl_3$ is only a slightly selective solvent for PS blocks. This could impart substantial mobility for both the PS blocks and P4VP/PMSSQ-P complex chains. During $CHCl_3$ vapor annealing the swollen PS blocks and P4VP/PMSSQ-P complexes repel one another and tend to organize into a well-defined structure. The cylindrical, microphase-separated structures are quite consistent with that predicated according to the self-consistent mean field theory (Table 1); therefore, it could be concluded the formation of the cylinders morphology was a thermodynamics-controlled process.

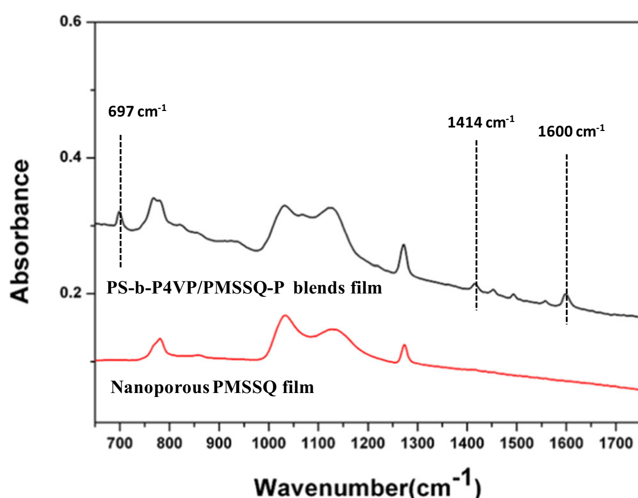


**Fig. 5** FTIR spectrum of the self-assembled PS-*b*-P4VP/PMSSQ-P blends thin film and resultant nanoporous PMSSQ thin film after annealing at 350 °C and 450 °C, successively, for 0.5 h at each temperature

Figure 3 shows the AFM height images of the PS-*b*-P4VP/PMSSQ-P blends thin films annealed in $CHCl_3$ as a function of PS-P4VP loading. For the PS-*b*-P4VP/PMSSQ-P thin films with PS-P4VP loadings ranging from 30 wt% to 60 wt%, an oriented cylinder morphology was obtained (Figs. 3a-d). The formation mechanism was discussed above. However, when the PS-P4VP loading was further increased, to 70 wt% and 80 wt%, the AFM image demonstrated a relatively flat surface (Figs. 3e-f), indicating no obvious microphase-separation occurred. For the blends thin films with higher weight content of PS-P4VP, of 70% and above (that is to say, the relative content of PMSSQ-P was 30% or less), the $CHCl_3$ vapor was highly miscible with the PS blocks and the P4VP/PMSSQ-P complexes, leading to a decrease of segregated repulsion between the two components. Therefore, it was difficult to achieve microphase-separation for these PS-*b*-P4VP/PMSSQ-P blends thin films.

Based on the above results, the self-assembled PS-*b*-P4VP/PMSSQ-P blends thin films with PS-*b*-P4VP loading ranging from 30 wt% to 60 wt% were further thermally treated at 25 °C, 50 °C, 80 °C, 100 °C, and 120 °C for 30 min sequentially, to complete the conversion of PMSSQ-P to PMSSQ and subsequent decompostion of PS-*b*-P4VP to prepare nanoporous PMSSQ thin films. Figure 4 shows the TGA curves of pure PMSSQ-P and the PS-*b*-P4VP block copolymer. It can be seen that PS-*b*-P4VP decomposed between 330 °C and 450 °C, while PMSSQ-P had only a 15%–20% weight loss below 300 °C which could be attributed to condensation among the Si-OH groups. The results mean that as the pyrolysis of the PS-*b*-P4VP occurred, the condensation and cross-linking reaction of PMSSQ-P almost finished to maintain the stable pore structures. The complete removal of PS-*b*-P4VP for the PS-*b*-P4VP/PMSSQ hybrid films during annealing at 350 °C and 450 °C sequentially was confirmed by FTIR analysis. As shown in Fig. 5, disappearance of the peaks at 697 $cm^{-1}$, 1414 $cm^{-1}$, and 1600 $cm^{-1}$, corresponding to the carbon-nitrogen distortion vibrations, and carbon-

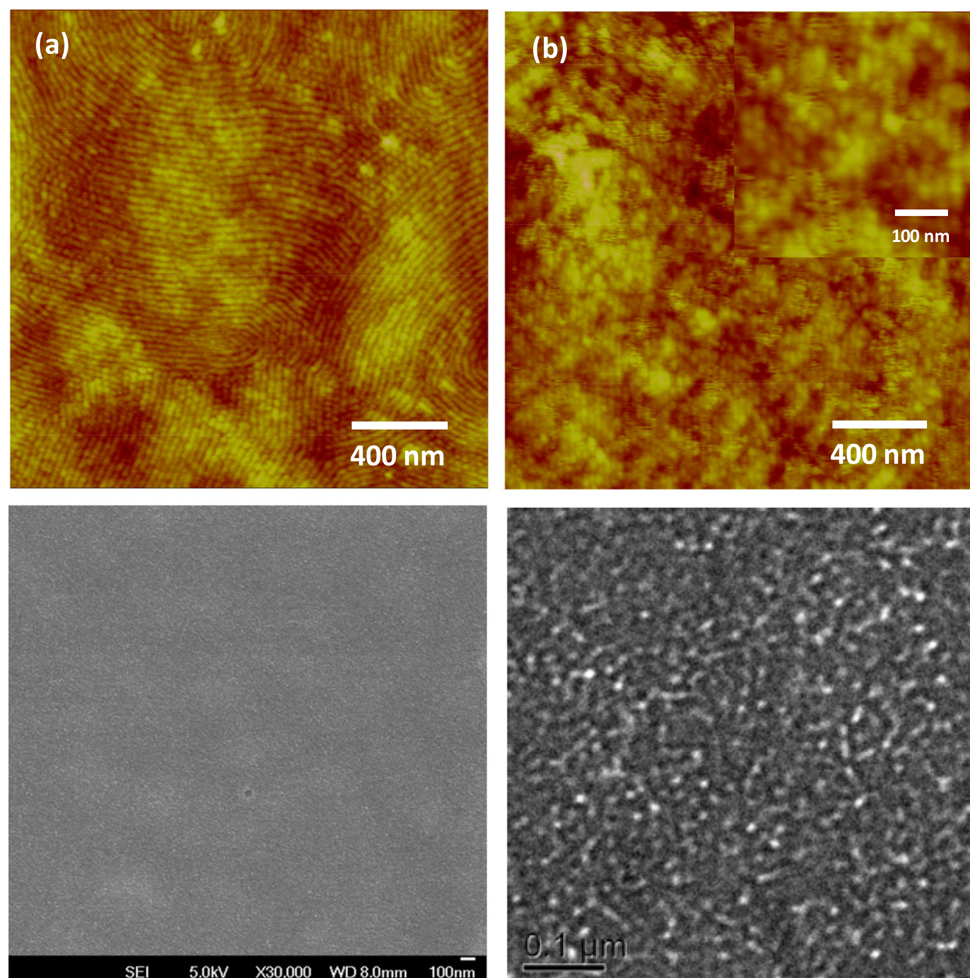


**Fig. 6** AFM height images of (**a**) self-assembled PS-*b*-P4VP/PMSSQ-P blends thin films with PS-*b*-P4VP loading of 50 wt%, and (**b**) corresponding nanoporous PMSSQ thin films after removal of PS-*b*-P4VP. (**c**) SEM image and (**d**) TEM image of the nanoporous PMSSQ thin films. Inset in (**b**): enlarged AFM height image of the nanoporous PMSSQ thin film

nitrogen stretching vibrations of the pyridine rings and the carbon-carbon stretching vibrations of the benzene rings in the PS-b-P4VP block copolymer, respectively, revealed the complete decomposition of the PS-*b*-P4VP block copolymer.

Figure 6b shows the AFM image of the nanoporous PMSSQ thin film prepared from the self-assembled PS-*b*-P4VP/PMSSQ-P blends thin films with 50 wt% PS-b-P4VP loading, after decomposition of the PS-*b*-P4VP block copolymer. Compared to the initial self-assembled PS-*b*-P4VP/PMSSQ-P blends thin films (Fig. 6a), the fingerprint-type orientation disappeared and the cylindrical morphology changed into disordered spherical structures. This is probably because the curing process and pyrolysis of PS-*b*-P4VP had an impact on the self-assembled structures. Although the thermal curing of the self-assembled PS-*b*-P4VP/PMSSQ-P thin films was carried out between 25 °C and 120 °C, which is below the glass transition temperature ($T_g$, 141 °C) of the P4VP blocks in the PS-b-P4VP (see Inset of Fig. 4), actually, the condensation and cross-linking reactions of the Si-OH were not achieved completely [38]. The subsequent porogen pyrolysis imparted slight mobility to the PS-*b*-P4VP/PMSSQ-P chains and gave rise to the transformation of the self-assembled structures. Although the prepared nanoporous PMSSQ thin films did not possess similar oriented morphology as the self-assembled films, it presented a uniform spherical morphology without any large size or other aggregation structures (Fig. 6b). The SEM image of Fig. 6c further confirms the homogeneity of the film over a large area. TEM was used to study the porous structures of PMSSQ thin film, as shown in Fig. 6d. It can be seen that closed nanoscale pores, with a diameter ~15 nm, were formed in the PMSSQ thin film.

For comparison purpose, porous PMSSQ films were prepared from the spin-cast PS-*b*-P4VP/PMSSQ-P thin films without any solvent annealing. As shown in Fig. 7, the prepared porous PMSSQ thin film was inhomogeneous, with randomly shaped particles, aggregations and large interconnected pores. The conspicuous difference between the two prepared porous PMSSQ thin films demonstrated the self-assembly behavior of the PS-*b*-P4VP/PMSSQ-P upon solvent annealing played an important role in the formation of the homogenous porous structures.

Table 2 summarizes the refractive indices of the nanoporous PMSSQ films. It can be seen that the refractive index of the nanoporous PMSSQ thin films linearly decreased

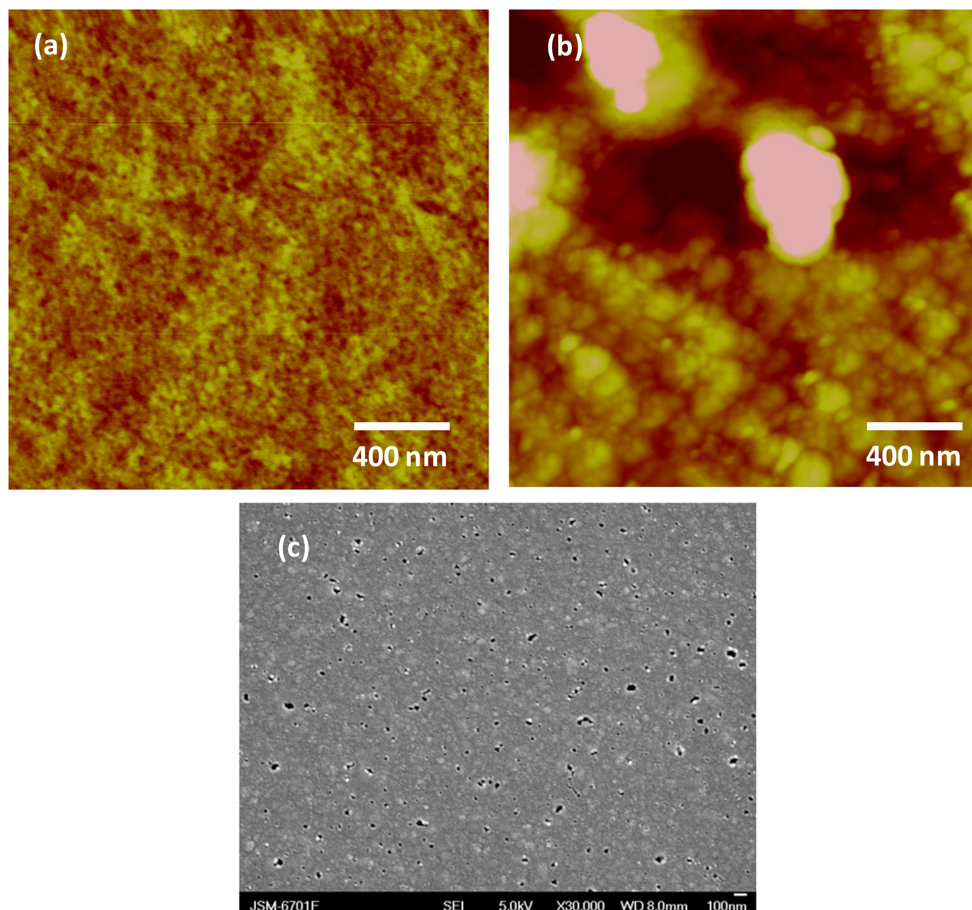


**Fig. 7** **a** AFM height image of spin-coating PS-*b*-P4VP/PMSSQ-P blends thin films with PS-*b*-P4VP loading of 50 wt%; **b** AFM height image and (**c**) SEM image of corresponding nanoporous PMSSQ thin films after removal of PS-*b*-P4VP

from 1.358 to 1.131 as the PS-b-P4VP loading was increased from 0 to 60 wt%. The porosities and dielectric constants of the PMSSQ thin films were calculated from the refractive indices accrording to the Lorentz–Lorenz and Maxwell equations [24, 25], and also listed in Table 2. The results indicated the porosities and dielectric constants of the PMSSQ films could be adjusted by changing the PS-*b*-P4VP wt% in the PS-*b*-P4VP/PMSSQ-P blends films. As the PS-*b*-P4VP loading increased from 30 wt% to 60 wt%, as shown in Table 2, the dielectric constant of the films decreased from 1.75 to an ultralow value of 1.41, significantly lower than that of the dense PMSSQ films (2.03). The results indicates that the incorporation of nanopores effectively reduced the dielectric constant of the PMSSQ films, making it have potential applications in microelectronic devices.

## Conclusions

Nanoporous PMSSQ films were prepared based on the self-assembly of PS-*b*-P4VP/PMSSQ-P blends thin films. A simple process of solvent annealing was used to produce the self-assembled structures of the PS-*b*-P4VP/PMSSQ-P blends thin films. By simply exposing to $CHCl_3$ vapor at room temperature,

**Table 2** Refractive index, porosity and dielectric constant of nanoporous PMSSQ films prepared from PS-*b*-P4VP/PMSSQ-P blends films with different PS-*b*-P4VP wt%

| PS-*b*-P4VP loading (wt%) | Refractive Index | Porosity [a] | Dielectric Constant [b] |
|---|---|---|---|
| 0 | 1.358 | – | 2.03 |
| 30% | 1.261 | 25.1% | 1.75 |
| 40% | 1.221 | 36.0% | 1.64 |
| 50% | 1.172 | 49.6% | 1.51 |
| 60% | 1.131 | 61.2% | 1.41 |

[a] Determined according to Lorentz–Lorenz equation [24]

[b] Determined according to Maxwell equation [25]

fingerprint-type microphase-separated structures were achieved for the PS-*b*-P4VP/PMSSQ-P blends thin films with PS-*b*-P4VP loading ranging from 30 wt% to 60 wt%. The self-assembled thin films were thermally treated to a sequence of elevated temperatures up to 120 °C to complete the conversion of PMSSQ-P to PMSSQ. Subsequently, nanoporous PMSSQ films were obtained by the thermal decomposition of PS-*b*-P4VP at 350 °C and 450 °C, sequentially. Although the prepared nanoporous PMSSQ thin films did not possess similar oriented morphology to the self-assembled films, they presented a homogenous spherical morphology with closed pores and a uniform size distribution over large areas. The porosity and dielectric properties of the homogenous nanoporous PMSSQ could be adjusted by the weight content of PS-*b*-P4VP in the PS-*b*-P4VP/PMSSQ-P blends. The incorporation of nanopores effectively reduced the dielectric constant of PMSSQ films, making it have potential application in microelectronic devices.

**Acknowledgements** The authors would like to acknowledge the financial support of the Nature Science Foundation of China (NSFC) (Grant No. 51403219), National Natural Science Foundation of China-Aerospace Science and Technology Corporation of China Aerospace Advanced Manufacturing Technology Research Joint Fund (U1637205), and Beijing Key Laboratory of Long-life Technology of Precise Rotation and Transmission Mechanisms (BZ0388201701).

## References

1. Semiconductor Industry Association. International technology roadmap for semiconductors, 2011 edition. International SEMATECH, Austin TX, 2011
2. Volksen W, Miller RD, Dubois G (2010) Low dielectric constant materials. Chem Rev 110:56–110
3. Treichel H (2001) Low dielectric constant materials. J Electron Mater 30:290–298
4. Vedamurthy T, Murugesan M (2018) In-situ PMMA modified p-cresol resin-nylon 6 polymer blends and evaluation of their hydrophobic and dielectric properties. J Polym Res 25:209
5. Homma T (1998) Low dielectric constant materials and methods for interlayer dielectric films in ultra large-scale integrated circuit multilevel interconnections. Mater Sci Eng R 23:243–285
6. Wang C, Wang TM, Wang QH (2013) Low-dielectric, nanoporous polyimide thin films prepared from block copolymer templating. Express Polym Lett 7:667–672
7. King SW, Jacob D, Vanleuven D, Colvin B, Kelly J, French M, Bielfeld J, Dutta D, Liu M, Gidley D (2012) Film property requirements for hermetic low-k a-SiOxCyNz:H dielectric barriers. ECS J Solid State Sci Technol 1:115–122
8. Lee LH, Chen WC, Liu WC (2002) Structural control of oligomeric methyl silsesquioxane precursors and their thin-film properties. J. Polym. Sci. A Polym. Chem. 40:1560–1571
9. Kim CS, Jeong HD (2008) What originates the dielectric permittivity of silicate-Silsesquioxane hybrid thin films? J Phys Chem B 112: 16257–16260
10. Jahromi S, Mostert B (2004) Templating nanoporosity in polyorganosilicates using reactive dendrimers. Macromolecules 37:2159–2162
11. Lee B, Park YH, Hwang YT, Oh W, Yoon J, Ree AM (2005) Ultralow-k nanoporous organosilicate dielectric films imprinted with dendritic spheres. Nat Mater 4:147–151
12. Lee B, Oh W, Hwang Y, Park YH, Yoon J, Jin KS, Heo K, Kim J, Kim KW, Ree M (2005) Imprinting well-controlled nanopores in organosilicate dielectric films: triethoxysilyl-modified six-armed poly(ϵ-caprolactone) and its chemical hybridization with an organosilicate precursor. Adv Mater 17:696–701
13. Magbitang T, Lee VY, Miller RD, Toney MF, Lin Z, Briber RM, Kim HC, Hedrick JL (2005) Templating organosilicate vitrification using unimolecular self-organizing polymers: evolution of morphology and nanoporosity development with network formation. Adv Mater 17:1031–1035
14. Kim JS, Kim HC, Lee B, Ree M (2005) Imprinting of nanopores in organosilicate dielectric thin films with hyperbranched ketalized polyglycidol. Polymer 46:7394–7402
15. Huang QR, Kim HC, Huang E, Mecerreyes D, Hedrick JL, Volksen W, Frank CW, Miller RD (2003) Miscibility in organic/inorganic hybrid nanocomposites suitable for microelectronic applications: comparison of modulated differential scanning calorimetry and fluorescence spectroscopy. Macromolecules 36:7661–7671
16. Yang S, Mirau PA, Pai CS, Nalamasu O, Reichmanis E, Lin EK, Lee HJ, Gidley DW, Sun J (2001) Molecular templating of nanoporous ultralow dielectric constant (≈1.5) organosilicates by tailoring the microphase separation of triblock copolymers. Chem Mater 13:2762–2764
17. Yang S, Mirau PA, Pai CS, Nalamasu O, Reichmanis E, Pai JC, Obeng YS, Seputro J, Lin EK, Lee HJ, Sun J, Gidley DW (2002) Nanoporous ultralow dielectric constant organosilicates templated by triblock copolymers. Chem Mater 14:369–374
18. Chang Y, Chen CY, Chen WC (2004) Poly(methyl silsesquioxane) amphiphilic block copolymer hybrids and their porous derivatives: poly(styrene-block-acrylic acid) and poly(styrene-block-3 trimethoxysilylpropyl methacrylate). J Polym Sci B Polym Phys 42:4466–4477
19. Yang CC, Wu PT, Chen WC, Chen HL (2004) Low dielectric constant nanoporous poly(methyl silsesquioxane) using poly (styrene-block-2-vinylpyridine) as a template. Polymer 45:5691–5702
20. Lee CH, Chen WC, Hsu JY, Chen HL (2007) Effect of molecular architecture of copolymer template on the morphology of mesoporous methylsilsesquioxane. Polymer 48:3546–3554
21. Yang YY, Yang CC (2008) Preparation of nanoporous poly(methyl silsesquioxanes) films using PS-b-P4VP as template. J Nanosci Nanotechnol 8:1537–1544
22. Lee B, Yoon J, Oh W, Hwang Y, Heo K, Jin KS, Kim J, Kim KW, Ree M (2005) In-situ grazing incidence small-angle X-ray scattering studies on nanopore evolution in low-k organosilicate dielectric thin films. Macromolecules 38:3395–3405
23. Lee LH, Chen WC, Liu WC (2002) Structural control of oligomeric methyl SilsesquioxanePrecursors and their thin-film properties. J Polym Sci A Polym Chem 40:1560–1571
24. Oh W, Hwang YH, Park YH, Ree M, Chu SH, Char K, Lee JK, Kim SY (2003) Optical, dielectric and thermal properties of nanoscaled films of polyalkylsilsesquioxane composites with star-shaped poly(ε-caprolactone) and their derived nanoporous analogues. Polymer 44:2519–2527
25. Matsumoto T (1999) Nonaromatic polyimides derived from cycloaliphatic monomers. Macromolecules 32:4933–4939
26. Wang QH, Wang C, Wang TM (2012) Nanophase-separated structuresof hydrogen-bonded interpolymer complexes of AB block copolymer/Chomopolymer in thin film with variable blending composition upon solvent annealing. J Macromol Sci B 51: 671–684
27. Dobrosielska K, Wakao S, Takano A, Matsushita Y (2008) Nanophase-separated structures of AB block copolymer/C

homopolymer blends with complementary hydrogen-bonding interactions. Macromolecules 41:7695–7698
28. Dobrosielska K, Wakao S, Suzuki J, Noda K, Takano A, Matsushita Y (2009) Effect of Homopolymer molecular weight on nanophase-separated structures of AB block copolymer/C Homopolymer blends with hydrogen-bonding interactions. Macromolecules 42: 7098–7102
29. Matsen MW, Bates FS (1996) Unifying weak- and strong-segregation block copolymer theories. Macromolecules 29:1091–1098
30. Hou XD, Li QB, Cao A (2014) Solvent annealing-induced micro-phase-separation of polystyrene-b-polylactide block copolymer aimed at preparation of ordered nanoparticles/block copolymer hybrid thin film. J Polym Res 21:491
31. Mao H, Li HF, Shang YR, Li JQ, Lu CH, An LJ, Jiang SC (2012) Solvent vapor induced structural evolution of micelle clusters and square slices that form in PS-b-PEO solutions. J Polym Res 19:11
32. Guo R, Huang HY, Chen YZ, Gong YM, Du BY, He TB (2008) Effect of the nature of annealing solvent on the morphology of diblock copolymer blend thin films. Macromolecules 41:890–900
33. Wang C, Wang TM, Wang QH (2010) Solvent annealing assisted self-assembly of hydrogen-bonded interpolymer complexes of AB block copolymer/C homopolymer in thin film. Polymer 51:4836–4842
34. Park S, Wang JY, Kim B, Chen W, Russell TP (2007) Solvent-induced transition from micelles in solution to cylindrical microdomains in diblock copolymer thin films. Macromolecules 40:9059–9063
35. Li Y, Wang X, Sanchez IC, Johnston KP, Green PF (2007) Ordering in asymmetric block copolymer films by a compressive fluid. J Phys Chem B 111:16–25
36. Zoelen WV, Asumaa T, Ruokolainen J, Ikkala O, Brinke GT (2008) Phase behavior of solvent vapor annealed thin films of PS-b-P4VP(PDP) supermolecules. Macromolecules 41:3199–3208
37. Lee W, Zhang X, Briber RM (2010) A simple method for creating nanoporous block-copolymer thin films. Polymer 51:2376–2382
38. Wang CY, Shen ZX, Zheng JZ (2001) High-temperature properties of a low dielectric constant organic spin-on glass for multilevel interconnects. Appl Spectrosc 55:1347–1351